

Velocity Profile Development and Friction in Compressible Micro-Flows

Marco Cavazzuti^{1,a)}, Mauro A. Corticelli¹ and Tassos G. Karayiannis²

¹*Dipartimento di Ingegneria “Enzo Ferrari”, Università degli Studi di Modena e Reggio Emilia, via P. Vivarelli 10, 41125 Modena, Italy*

²*Department of Mechanical and Aerospace Engineering, Brunel University London, Uxbridge, Middlesex UB8 3PH, United Kingdom*

^{a)}Corresponding author: marco.cavazzuti@unimore.it

Abstract. From Poiseuille theory, it is known that incompressible laminar fully-developed flow of a Newtonian fluid in a constant cross-section channel is characterised by steady parabolic velocity profiles after a fully-developed flow condition is attained. In turbulent fully-developed flow the velocity profiles are non-parabolic and become more flat for higher Reynolds numbers. When the incompressible hypothesis does not hold, as in the case of high velocity ideal gas flow, the velocity profile becomes flatter, as if more turbulent, due to the superposition of compressibility and turbulence effects, if applicable. This is typical in micro-channel flows, where pressure gradients are high and the gas is rapidly accelerating, eventually up to the sound velocity. As the flow accelerates the effects of compressibility grow stronger and the velocity profile keeps changing shape. The radial velocity component does not zero as in fully-developed flow but reverses after the entrance effects have damped out and grows with the Mach number. A net mass transfer toward the walls is thus generated making the velocity profile more flat. This affects the friction factor which is no longer constant, being proportional to the normal-to-wall velocity gradient, and needs to be evaluated. In the present work, the compressible friction factor is numerically investigated and correlations are proposed based on the velocity profile shape evolution as a function of the Mach number. This, together with other considerations on the velocity profile shape change, is shown to enhance the predictive capability of the Fanno theory for compressible flows.

INTRODUCTION

Micro-fluid flow represents an interesting research field which is attracting a growing interest due to a plethora of possible applications, mostly engendered by miniaturisation in several technological fields. One of the most promising is given by cooling in electronics [1] where the dissipated power densities are growing very rapidly and the need of simple and efficient local cooling systems is more and more stringent.

Unfortunately, experiments at such small scales are often error prone [2], if possible at all, so that contrasting opinions have been drawn in the recent literature on the understanding of the fundamental physics governing this kind of flows [3]. Micro-fluid flow is usually characterised by steep pressure gradients being dominated by friction [4]. As a consequence, when the fluid involved is a gas the effects of compressibility must be carefully addressed.

Analytical models for confined compressible flows were derived by Fanno and Rayleigh [5], based on differential conservation equations. For given boundary conditions, these models allow the closed form solution of the main flow characteristics (e.g. pressure, temperature, velocity, Mach number) in constant cross-section channels for the non-isentropic adiabatic (Fanno), or the isentropic diabatic (Rayleigh) cases. Focusing on Fanno, similar considerations are possible regarding as with the Rayleigh theory, flow characteristics at any point along the channel can be predicted as function of the Mach number and the friction factor once the characteristics are known at another location. This analytical tool, however, does not specify how friction should be evaluated, and canonical incompressible correlations [6] assuming constant friction in pipes are found to be inaccurate when compressibility is non-negligible.

Compressibility acts by deforming the velocity profile in the channel cross-sections. In particular, in [7] it is found that the profile becomes more flat for larger Mach and Reynolds numbers, the latter having an influence only in the case of turbulent flow. Compared to the well-known laminar incompressible parabolic profile derived from the

Poiseuille theory [8], flatter profiles result in altered velocity gradients at the wall and thus, by definition, in larger wall shear stresses and growing friction factors. In the literature, the evaluation of the compressible friction factor was addressed in [9] for the laminar case and in [10] for turbulent flow. These works are based on pressure and temperature experimental measurements and do not deal with the local velocity profile change in shape.

In addition, the average dynamic pressure and the bulk temperature are also affected by the velocity profile shape. These quantities are necessary for the proper evaluation of the flow characteristics starting from the boundary conditions that are better given in terms of total pressure and total temperature at the channel extremities. A detailed investigation of the velocity profiles is thus required for improving the predicting capability of the Fanno analytical tool. Due to the scale of the problem, such an investigation cannot be carried out experimentally and must rely on numerical tools.

In the present work, the compressible flow in micro-channels is investigated by means of CFD, and velocity profiles at different sections are analysed. The shape of the velocity profile is correlated to the change in friction factor, average dynamic pressure, and bulk temperature. The correlations provide suitable correction terms for the analytical model, and a mean for the evaluation of the compressible friction factor. This makes it possible to perform fast and accurate predictions of the compressible flow characteristics in micro-channels where the standard analytical model would lose in accuracy. Both laminar and turbulent flows, and both circular and parallel-plate cross-section channels are addressed.

FANNO FLOW THEORETICAL BACKGROUND AND NUMERICAL MODEL

Fanno theory provides a rigorous analytical model for the prediction of adiabatic compressible flow in constant cross-section channels. Starting from the definitions of speed of sound for an ideal gas c and of Mach number Ma

$$Ma = \frac{U}{c} = \frac{U}{\sqrt{\gamma R_g T}} \quad (1)$$

and the ideal gas law

$$p = \rho R_g T \quad (2)$$

the model is based on the conservation equations of mass

$$\dot{m} = \rho U A \quad (3)$$

momentum

$$F_v = \Delta(p + \rho U^2) A = - \int P \tau_w dx \quad (4)$$

and energy

$$c_p T + \frac{U^2}{2} = h_0 \quad (5)$$

where γ is the heat capacity ratio, R_g the specific gas constant, \dot{m} the mass flow rate, A the channel cross-section area, F_v the resultant viscous forces, P the channel cross-section perimeter, τ_w the wall shear stress, c_p the specific heat at constant pressure, and h_0 the stagnation specific enthalpy. By differentiating, and with a few algebraic steps, the equations above can be written in differential form where the main flow characteristics such as pressure p , temperature T , velocity U , density ρ , and the Mach number Ma can be written as functions of the Mach number and the friction factor, *e.g.*

$$\frac{dMa}{Ma} = \frac{\gamma Ma^2 \left(1 + \frac{\gamma-1}{2} Ma^2\right) f dx}{2(1 - Ma^2) D_h} \quad (6)$$

where f is the Darcy friction factor defined as

$$f = \frac{8\tau_w}{\rho U^2} \quad (7)$$

However, the Fanno theoretical model does not specify how to assess friction, and it is known that canonical formulas hold only for incompressible flows.

Since the friction factor is not constant along the channel and the Mach number differential is a function of

the Mach number itself, the compressible flow is better solved by recurring to a fine 1D spatial discretization of the channel in order to follow closely the local friction factor variation, and through an iterative shooting technique where the Mach number at the channel inlet is guessed for given upstream boundary conditions up to when downstream boundary conditions are met. Such a numerical model has been developed in python language featuring temperature-dependent fluid thermal properties, and with stagnation pressure and temperature boundary conditions. As such, a mean for the estimation of the compressible friction factor is needed for attaining accurate flow predictions. As the boundary conditions are more conveniently given at stagnation, means for evaluating the dynamic portions of pressure and temperature are also needed. Being the numerical model developed 1D, all the quantities extending over the cross-section area are to be intended as area-weighted-average (awa) values if referring to pressure and velocity and as mass-weighted-average (mwa), or bulk, values in case of temperature and temperature-dependent quantities (*e.g.* the thermal properties).

Locally, the dynamic pressure p_d and the dynamic temperature T_d are defined as

$$p_d = \frac{\rho U^2}{2} \quad (8)$$

$$T_d = \frac{U^2}{2c_p} \quad (9)$$

By integrating, their average values over the cross-section cannot be expressed in the same form, *i.e.* in terms of the average quantities available from the 1D model, without introducing fitting coefficients g

$$p_{d,awa} = \frac{\int_A \frac{\rho U^2}{2} dA}{\int_A dA} = g_p \frac{\rho_{mwa} U_{awa}^2}{2} \quad (10)$$

$$T_{d,mwa} = \frac{\int_A \frac{\rho U^3}{2c_p} dA}{\int_A \rho U dA} = g_T \frac{U_{awa}^2}{2c_{p,mwa}} \quad (11)$$

Correlations able to predict the compressible friction factor in a channel and the g coefficients introduced above would fill the gap by providing the required numerical tools for enhancing the predictive capability of the 1D Fanno flow model described. These tools must rely on a detailed analysis of the velocity profiles and of their change in shape with compressibility.

Due to the typical micro-scale of the problem, this analysis cannot be carried out experimentally and must rely on numerical tools such as CFD simulations. Friction and the fitting coefficients can be evaluated at each section as

$$f = \frac{8\tau_w}{\rho_{mwa} U_{awa}^2} \quad (12)$$

$$g_p = \frac{2p_{d,awa}}{\rho_{mwa} U_{awa}^2} \quad (13)$$

$$g_T = \frac{2c_{p,mwa} T_{d,mwa}}{U_{awa}^2} \quad (14)$$

where all the terms on the right-hand side of the equations are available from the CFD simulation post-processing. A detailed analysis of the velocity profile evolution along the channel from post-processing is also possible.

CFD SIMULATIONS SETUP

Simulations were carried out for circular and parallel-plate cross-sections. The mesh chosen was axisymmetric or planar, depending on the cross-section type, and fully structured. Large plenums were modelled at the channel extremities so that boundary conditions were set where static and total quantities almost coincide with regard to pressure and temperature. The mesh size was adapted from case to case in order to limit the maximum y^+ value, and ranged between 5×10^5 and 5×10^6 elements. An off-scale mesh example having 500 elements is shown in Fig. 1.

As the flow is highly compressible a coupled CFD solver is needed for the simulations: Ansys Fluent was chosen

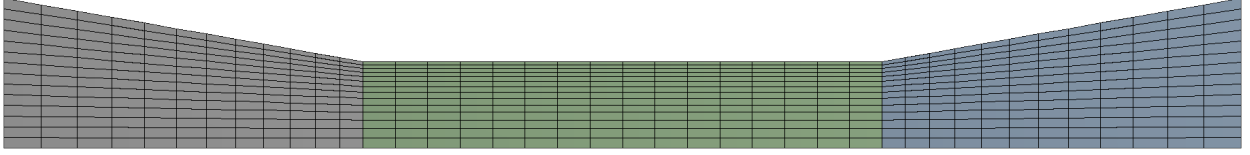


FIGURE 1. Off-scale mesh example.

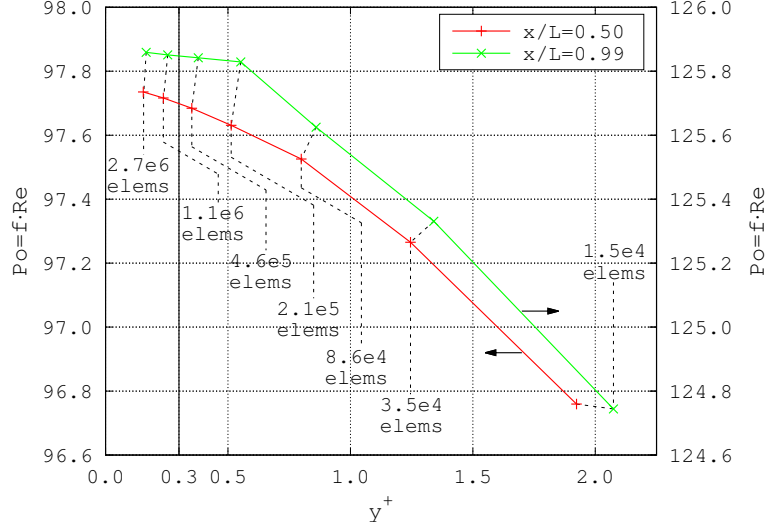


FIGURE 2. Results of the CFD mesh convergence study: y^+ vs Poiseuille number Po . The vertical line indicates the y^+ constraint required for mesh acceptance. The arrows indicate the reference abscissae axis for each line in the plot. Lines are drawn for two different longitudinal locations in the channel.

for the purpose. Boundary conditions were total pressure and temperature at the inlet, static pressure at the outlet, and no-slip at the wall. Second-order discretization schemes were chosen, together with SST $k-\omega$ turbulence model. The set of equations solved was the following

$$\left\{ \begin{array}{ll} \nabla \cdot (\rho \mathbf{U}) = 0 & \text{Mass conservation} \\ \nabla \cdot (\rho \mathbf{U} \mathbf{U}) = -\nabla p + \nabla \cdot \boldsymbol{\tau} & \text{Momentum conservation} \\ \nabla \cdot (\rho \mathbf{U} (E + p/\rho)) = \nabla \cdot (\lambda_e \nabla T + \boldsymbol{\tau} \cdot \mathbf{U}) & \text{Energy conservation} \\ \nabla \cdot (\rho \mathbf{U} k) = \nabla \cdot (\Gamma_k \nabla k) + G_k - Y_k & \text{Transport of } k \\ \nabla \cdot (\rho \mathbf{U} \omega) = \nabla \cdot (\Gamma_\omega \nabla \omega) + G_\omega - Y_\omega + Z_\omega & \text{Transport of } \omega \end{array} \right. \quad (15)$$

where $\boldsymbol{\tau}$ is the stress tensor, E the total energy, λ_e the effective thermal conductivity, $\boldsymbol{\tau} \cdot \mathbf{U}$ the viscous heating term, k the turbulence kinetic energy, and ω the turbulence specific dissipation rate. The terms Γ , G , Y , and Z in the last two transport equations represent the effective diffusivity, the production, the dissipation, and the cross-diffusion of the turbulent quantities, respectively.

More than 90 CFD simulations were solved spanning Reynolds numbers in the laminar and in the turbulent regions ($0 \leq Re \leq 20000$), and Mach numbers in the subsonic region ($0 \leq Ma \leq 1$) for two cross-section types (circular and parallel-plate). The channels investigated had different hydraulic diameters ($100 \mu\text{m}$ for the laminar case, and $500 \mu\text{m}$ for the turbulent case), length-to-hydraulic diameter ratios α (either 100 or 500), stagnation temperatures T_0 (either 300 K or 500 K). The downstream stagnation pressure p_1 was set to 1 bar, and various values of the upstream stagnation pressure p_0 were used for each possible configuration in order to span the subsonic region.

A preliminary mesh convergence test led to the choice of a suitable mesh refinement level, chosen in order to grant a maximum $y^+ \leq 0.3$ under any circumstance. Maximum errors $\leq 0.5\%$ in the prediction of the friction factor were estimated from Richardson extrapolation [11]. An example of the mesh convergence study results is given in Fig. 2 for the laminar case. Similar plots were found for the turbulent case and are omitted for brevity.

During the simulations post-processing the velocity profile and the average flow characteristics needed to solve

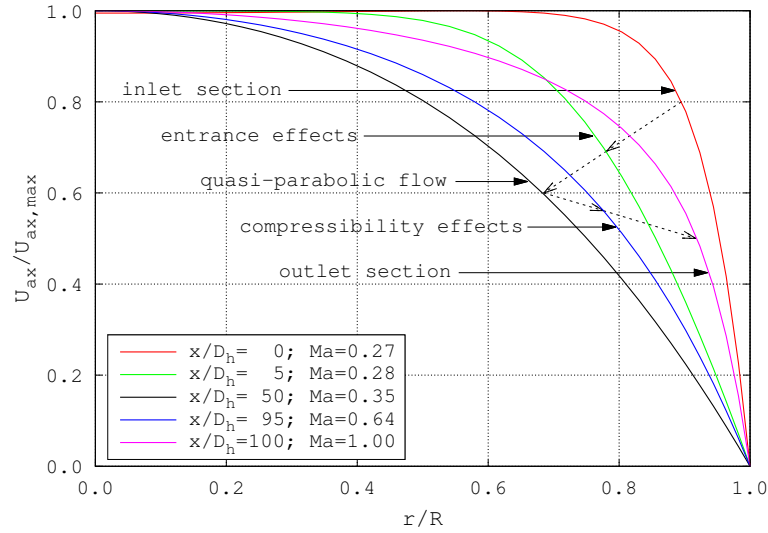


FIGURE 3. Compressible flow normalized axial velocity profile evolution from the inlet section to the outlet of a channel. The figure refers to the circular cross-section case with $D_h = 100 \mu\text{m}$, $\alpha = 100$, $T_0 = 500 \text{ K}$, $p_0 = 4 \text{ bar}$, $p_1 = 1 \text{ bar}$.

Eq. (12), (13) and (14) were extracted at 65 sections along the channel. Overall more than 6000 sections were extracted from the set of simulations performed. This set of sections was cleared from those where the entrance effects were still relevant, leaving approximately 3000 sections. This operation allowed the compressibility effects to be isolated from the developing flow entrance effects, avoiding any bias in the results of the processed data where the focus is on compressibility effects alone.

VELOCITY PROFILES EVOLUTION

At the inlet section of a channel the velocity profile is characterised by a rather flat shape, being the flow still far from developed. From there, the compressible profile shifts towards a more parabolic shape eventually becoming quasi-parabolic in case of laminar flow. The term “quasi” is used here since, strictly speaking, a perfectly parabolic velocity profile is achieved only in case of incompressible laminar flow, according to Poiseuille theory. In case of turbulent flow, instead, a transition to turbulence, characterised by flatter profiles, occurs shortly after the entrance section, before a quasi-parabolic velocity profile is attained. From there, as the Mach number increases due to the rapid flow acceleration caused by the large pressure drop, the velocity profile keeps changing in shape becoming more and more flat. This holds for both laminar and turbulent flows. Figure 3 shows the velocity profile evolution, from flat to parabolic and back to flat, moving from the channel inlet to the outlet section for a laminar choked-flow case. For these shape changes to occur it is necessary that mass is transferred towards the centre of the cross-section in a developing flow, and away from the centre as the Mach number grows.

By plotting the velocity profiles extracted from the CFD simulations it is noted that, besides on the cross-section type, the profile shape depends only on the Mach number for the case of laminar flow, and on the Mach and the Reynolds numbers for the case of turbulent flow. In fact, profiles characterised by the same nondimensional numbers and cross-section type are perfectly superimposable. The profile shapes are resumed in Fig. 4. Of course turbulent profiles are flatter than laminar ones. Besides, it is noted that the profiles become more flat with growing Mach and Reynolds numbers. The impact of the Reynolds number gradually fades as the number increases, on the contrary the impact of the Mach number grows as the number increases. The circular cross-section is characterised by flatter profiles, compared to the parallel-plate cross-section, for the same nondimensional numbers.

With regard to friction, Eq. (12) can be written in terms of the Poiseuille number Po as

$$Po = fRe = \frac{8D_h}{U} \frac{\partial U}{\partial n} \quad (16)$$

Flatter velocity profiles imply larger normal-to-wall velocity derivatives $\partial U/\partial n$ and thus larger Poiseuille numbers. The same could not be said for the friction factor: while friction always grows with the Mach number due to the

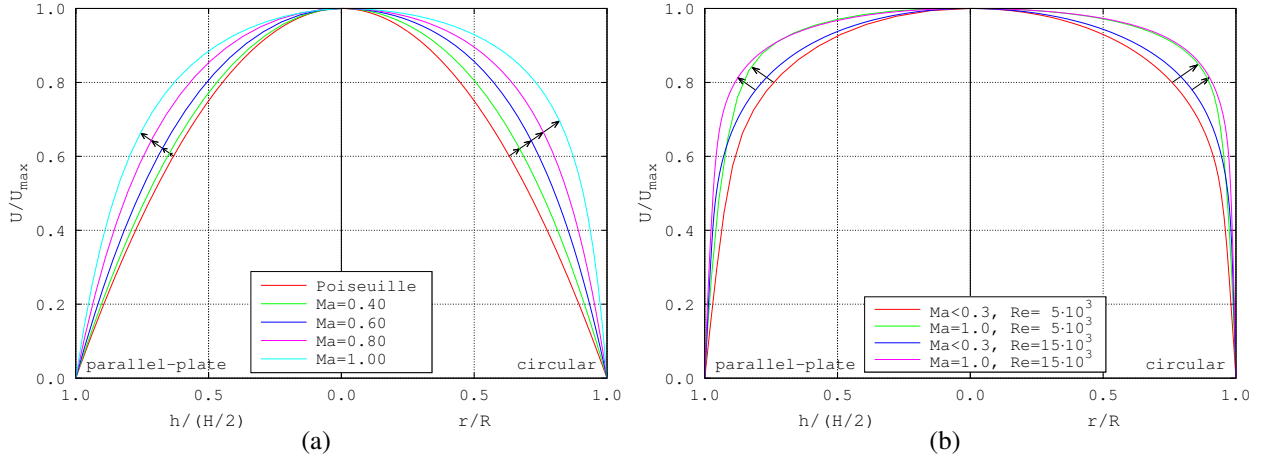


FIGURE 4. Normalized velocity profiles for different Mach and Reynolds numbers: (a) laminar case, (b) turbulent case. The arrows indicate the shape change for growing Mach numbers.

growth of the $\partial U/\partial n$ term, this is not true with respect to the Reynolds number since the growth of the normal-to-wall velocity derivative is overbalanced by the growth of the Reynolds number.

With regard to the fitting coefficients in Eq. (13) and (14), flatter profiles, whether due to the growth of the Mach or the Reynolds numbers, always bring to smaller values of the coefficients that, in the limit, tend to one for an ideal completely flat profile. The coefficients are thus better expressed by correlations that are function of the Mach number and, if the flow is turbulent, of the Reynolds number.

LAMINAR AND TURBULENT COMPRESSIBLE FLOW CORRELATIONS

It has been shown that the shape of the compressible velocity profile only depends on the Mach number and, in case of turbulent flow, on the Reynolds number. By evaluating Eq. (12), (13), and (14) over the set of 3000 sections extracted from the CFD simulations it is possible to map the friction factor and the fitting functions against the Mach and the Reynolds number. The result of this operation is shown in Fig. 5 for the laminar flow, and in Fig. 6 relatively to the turbulent flow in parallel-plate cross-section channels, similar plots can be drawn for the circular cross-section case but are omitted for brevity.

In Fig. 5a friction is substituted by the Poiseuille number, since this quantity is independent from the Reynolds number, and thus more meaningful for the laminar case. Two trends, one for the circular and the other for the parallel-plate cross-section case, are very clearly recognisable in Fig. 5. For the limiting case of incompressible flow ($Ma = 0$) the data match with the incompressible flow theory (*e.g.* $Po = 64$ for the circular, and $Po = 96$ for the parallel-plate cross-section case) with zero derivative with respect to the Mach number. As the Mach number is increased the data depart from the incompressible results more and more rapidly, with the fitting function approaching unity and the Poiseuille number growing. The variations are more pronounced for the circular cross-section case. All these results are in line with the previous analysis carried out on the velocity profile shape. The data spread in Fig. 5 is essentially null, and the data could be easily interpolated by polynomial functions attaining very low interpolation errors. From interpolation, the following correlations, valid for $0 \leq Ma \leq 1$, could be derived

$$Po_{\text{lam}}(Ma) = \begin{cases} 64 \left(1 + 0.653 Ma^2 + 2.809 Ma^3 - 5.311 Ma^4 + 4.157 Ma^5 \right) & \text{circular cross-section} \\ 96 \left(1 + 0.153 Ma^2 + 2.632 Ma^3 - 4.685 Ma^4 + 3.669 Ma^5 \right) & \text{parallel-plate cross-section} \end{cases} \quad (17)$$

$$g_{p,\text{lam}}(Ma) = \begin{cases} 4/3 - 0.318 Ma^2 + 0.118 Ma^3 & \text{circular cross-section} \\ 6/5 - 0.0530 Ma^2 - 0.0524 Ma^3 & \text{parallel-plate cross-section} \end{cases} \quad (18)$$

$$g_{T,\text{lam}}(Ma) = \begin{cases} 2 - 1.250 Ma^2 + 0.578 Ma^3 & \text{circular cross-section} \\ 54/35 - 0.204 Ma^2 - 0.121 Ma^2 & \text{parallel-plate cross-section} \end{cases} \quad (19)$$

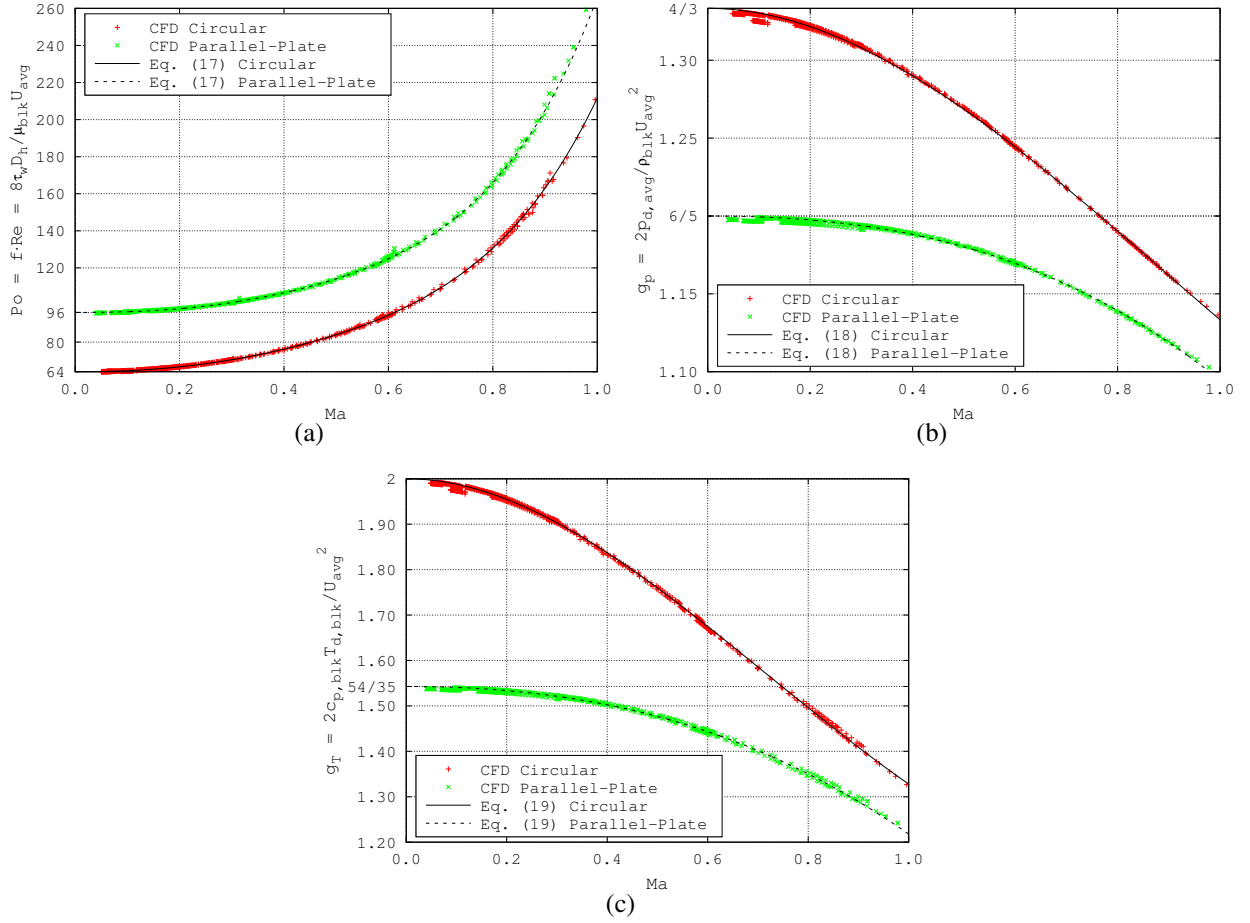


FIGURE 5. Laminar compressible Poiseuille number and fitting functions (dots) extracted from the CFD analyses as function of the Mach number, together with their interpolations (lines): (a) $Po(Ma)$, (b) $g_p(Ma)$, (c) $g_T(Ma)$. The + signs refer to the circular cross-section data, the × signs to the parallel-plate cross-section data.

The average interpolation error of the correlations above is always $<0.5\%$.

Figure 6 reports the results of the turbulent parallel-plate cross-section case as function of the Mach and the Reynolds number. It is shown how both the friction factor and the fitting functions decrease for growing Reynolds numbers. With regard to the Mach number, for a given Reynolds number, the trends are similar to those shown in Fig. 5, with the friction factor growing more and more rapidly with the Mach number, and the fitting functions approaching unity. At low values of the Mach number all the plotted functions depend only on the Reynolds number, being almost flat along the Mach number axis. This is in line with the fact that the effects of compressibility become noticeable only at higher Mach numbers. For this reason, correlations for the data in Fig. 6 are better given in terms of product of two terms: one modelling the incompressible behaviour in the low-Mach region and depending only on the Reynolds number, the other modelling the compressible behaviour in the high-Mach region as function of both the Mach and the Reynolds number and tending to one for Mach numbers approaching zero. It is noted that the incompressible friction factor that could be derived from Fig. 6a gradually tends to the well-known Blasius [12] and/or Colebrook-White smooth pipe correlations for growing Reynolds numbers. Also for the turbulent case, the data spread is almost null. The data are well interpolated by the following correlations valid in the $0 \leq Ma \leq 1$ and $0 \leq Re \leq 20000$ range

$$f_{\text{trb}}(Re, Ma) = \begin{cases} \left(\frac{3.159}{Re^{0.51-1.57 \cdot 10^{-6} Re}} \right) \left(1 + 49.75 \frac{Ma^{0.22}}{Re^{0.47}} \right) & \text{circular cross-section} \\ \left(\frac{3.744}{Re^{0.51-1.57 \cdot 10^{-6} Re}} \right) \left(1 + 82.58 \frac{Ma^{0.24}}{Re^{0.53}} \right) & \text{parallel-plate cross-section} \end{cases} \quad (20)$$

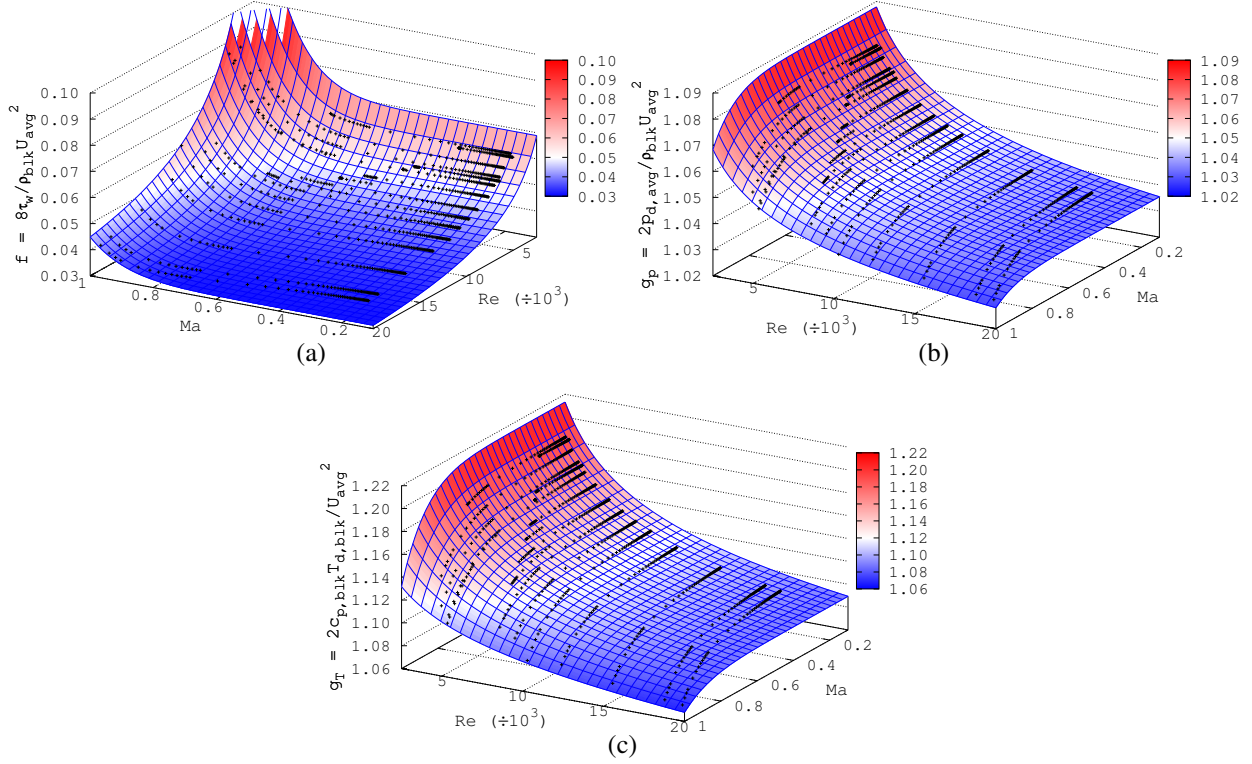


FIGURE 6. Turbulent compressible friction factor and fitting functions (dots) extracted from the CFD analyses as function of the Mach and the Reynolds numbers, together with their interpolations (surfaces): (a) $Po(Ma, Re)$, (b) $g_p(Ma, Re)$, (c) $g_T(Ma, Re)$. The data refer to the parallel-plate cross-section case (+ signs).

$$g_{p, \text{trb}}(Re, Ma) = \begin{cases} 1 + \left(\frac{2.789}{Re^{0.42}}\right) \left(1 - 0.658 \frac{Ma^{6.45}}{Re^{0.103}}\right) & \text{circular cross-section} \\ 1 + \left(\frac{2.672}{Re^{0.44}}\right) \left(1 - 0.276 \frac{Ma^{8.91}}{Re^{0.028}}\right) & \text{parallel-plate cross-section} \end{cases} \quad (21)$$

$$g_{T, \text{trb}}(Re, Ma) = \begin{cases} 1 + \left(\frac{6.603}{Re^{0.41}}\right) \left(1 - 1.230 \frac{Ma^{5.53}}{Re^{0.141}}\right) & \text{circular cross-section} \\ 1 + \left(\frac{5.591}{Re^{0.42}}\right) \left(1 - 2.188 \frac{Ma^{7.84}}{Re^{0.223}}\right) & \text{parallel-plate cross-section} \end{cases} \quad (22)$$

The average interpolation error of the correlations above is always $< 2\%$.

MODEL VALIDATION

The correlations in Eq. (17), (18), (19), (20), (21), and (22) for the evaluation of the friction factor and the dynamic pressure and temperature have been implemented in a 1D model solving the compressible flow in channels according to the Fanno theory. This model is referred to as the enhanced Fanno model. In parallel, another model where the correlations are not implemented is built, and is referred to as the standard Fanno model. In it the friction factor is predicted using the incompressible Colebrook-White formula for smooth pipes, and the dynamic pressure and temperature from Eq. (10) and (11) where $g_p = g_T = 1$.

The two models are tested against additional CFD simulations. For brevity, only the most critical case is discussed in the following in order to evaluate the performance of the enhanced model under a worst case scenario. The simulation data are chosen so that the flow is choked and turbulent, with a low Reynolds number ($Re \approx 4000$). This is an area where the curvature of the surfaces in Fig. 6 is high and the interpolation error of the correlations is maximum. The tested configuration is relative to a parallel-plate cross-section channel with hydraulic diameter $D_h = 0.4$ mm, length-to-hydraulic diameter ratio $\alpha = 1000$, stagnation temperature $T_0 = 600$ K, upstream stagnation pressure $p_0 = 9.0$ bar,

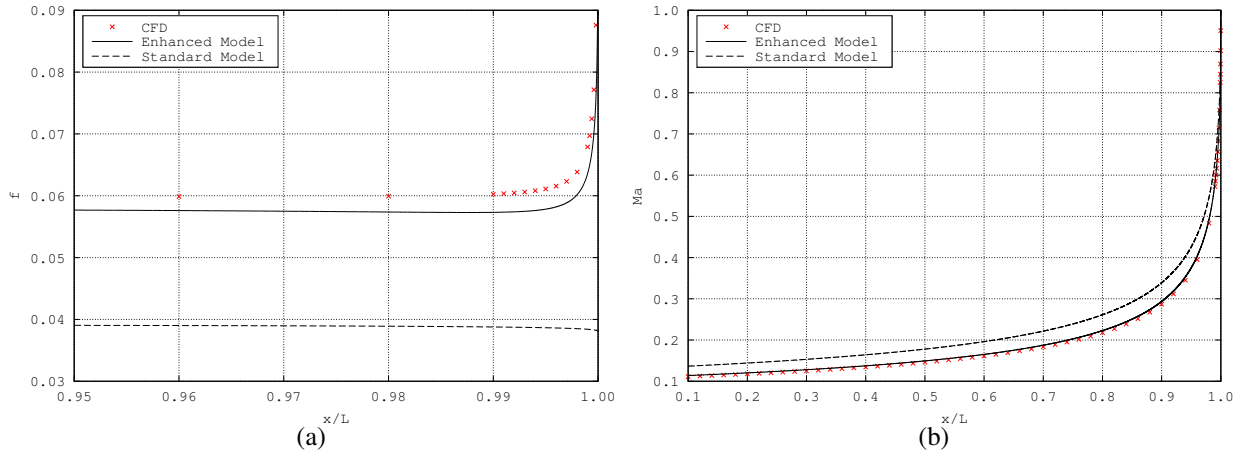


FIGURE 7. Model validation: CFD vs enhanced and standard 1D Fanno flow model results: (a) friction factor, (b) Mach number.

and downstream stagnation pressure $p_1 = 1.0$ bar. For a fairer comparison between the 1D models and the CFD results the developing flow region is skipped: the total pressure at the longitudinal coordinate of $x = 100D_h$ is read from CFD and imposed as boundary condition of the equivalent $\alpha = 900$ channel solved with the 1D models.

The results of the validation are shown in Fig. 7. The predictions made by the enhanced model replicate very closely the CFD results. The larger deviations, with respect to CFD, are found in the prediction of the friction factor with maximum errors of $\approx 3\%$ for the enhanced model, and errors between 35% and 70% for the standard model. The predicted mass flow rate along the channel is 54.67 g/s from CFD, 55.85 g/s (+2%) with the enhanced model, and 66.83 g/s (+22%) with the standard model.

CONCLUSIONS

Compressible flow velocity profiles in constant cross-section micro-channels have been investigated numerically by means of CFD simulations. The analysis took into consideration both the laminar and the turbulent flow cases, and the circular and the parallel-plate cross-sections.

It is noted that, due to the effects of compressibility, the velocity profile changes along the channel as a function of the local Mach number and, in case of turbulent flow, also of the local Reynolds number. In particular, the velocity profile becomes more flat for growing Mach and Reynolds numbers. This has a significant impact on the friction factor which is no longer constant but grows more and more rapidly as compressibility becomes important and the sonic flow velocity is approached at the channel outlet section. Not limited to this, also the average dynamic pressure and the bulk dynamic temperature at each section are affected by the shape of the velocity profile.

From the analysis of the velocity profile evolution in a series of CFD simulations, correlations have been extracted for the prediction of the friction factor, the dynamic pressure, and the bulk temperature in the range $0 \leq Ma \leq 1$ and $0 \leq Re \leq 20000$.

The correlations proposed, implemented in a 1D numerical model solving the compressible Fanno flow, are shown to allow much better predictions of the flow characteristics than the standard models where, due to the fact that the theory does not provide a mean for evaluating the friction variability, a constant friction factor is erroneously often assumed in the channel. The correlations, being based on the analysis of the velocity profile shape, give the 1D model a quasi-2D accuracy that otherwise would not be achievable.

The model proposed provides an accurate and fast tool for the design of compressible flow micro-channels in real-life applications. Due to the similarities among the Fanno and the Rayleigh theories, a model extension in order to include heat transfer effects is not expected to entail particular difficulties from the numerical point of view.

REFERENCES

- [1] M. J. Khol, S. I. Abdel-Khalik, S. M. Jeter, and D. L. Sadowski, *Int. J. Heat Mass Transf.* **48**, 1518–1533 (2005).
- [2] P. Rosa, T. G. Karayiannis, and M. W. Collins, *Appl. Therm. Eng.* **29**, 3447–3468 (2009).
- [3] G. Hetsroni, A. Mosyak, E. Pogrebnyak, and L. P. Yarin, *Int. J. Heat Mass Transf.* **48**, 1982–1998 (2005).
- [4] A. Cioncolini, F. Scenini, J. Duff, M. Szolcek, and M. Curioni, *Exp. Therm. Fluid Sci.* **74**, 49–57 (2016).
- [5] J. W. Strutt, *Proc. Roy. Soc. Lond. A* **84**, 247–284 (1910).
- [6] C. F. Colebrook and C. M. White, *Proc. Roy. Soc. Lond. A* **161**, 367–381 (1937).
- [7] M. Cavazzuti, M. A. Corticelli, and T. G. Karayiannis, *Therm. Sci. Eng. Progr.* **10**, 10–26 (2019).
- [8] J. L. Poiseuille, *Recherches expérimentales sur le mouvement des liquides dans les tubes de très-petits diamètres* (Imprimerie Royale, 1844).
- [9] Y. Asako, T. Pi, S. Turner, and M. Faghri, *Int. J. Heat Mass Transf.* **46**, 3041–3050 (2003).
- [10] C. Hong, T. Nakamura, Y. Asako, and I. Ueno, *Int. J. Heat Mass Transf.* **98**, 643–649 (2016).
- [11] P. Roache, *Annu. Rev. Fluid Mech.* **29**, 123–160 (1997).
- [12] P. R. H. Blasius, *Forschungsheft* **131**, 1–41 (1913).